Cusp aurora dependence on interplanetary magnetic field B_z

S. A. Fuselier,[1] H. U. Frey,[2] K. J. Trattner,[1] S. B. Mende,[2] and J. L. Burch[3]

Received 26 July 2001; revised 31 October 2001; accepted 31 October 2001; published 18 July 2002.

[1] The Imager for Magnetopause to Aurora Global Exploration (IMAGE) Spectrographic Imager (SI12) detects Doppler-shifted Lyman alpha emissions created by charge exchange and de-excitation of precipitating protons in the atmosphere. At high latitudes near local noon, emissions consistent with the location of the cusp foot point have distinct interplanetary magnetic field (IMF) dependence. For northward IMF a spot of emissions is observed poleward of the dayside auroral oval. By tracing the magnetic field lines from this spot using a model magnetosphere it is shown that the cusp foot point maps to a narrow region on the high-latitude magnetopause where antiparallel magnetic reconnection may be occurring. As the IMF turns southward, the spot merges into the auroral oval, producing a broad region of intense emissions centered near local noon. By tracing the magnetic field lines from this broad region using a model magnetosphere it is shown that the cusp foot point maps to a relatively broad region on the dayside magnetopause where component magnetic reconnection may be occurring. *INDEX TERMS:* 2736 Magnetospheric Physics: Magnetosphere/ionosphere interactions; 2455 Ionosphere: Particle precipitation; 7835 Space Plasma Physics: Magnetic reconnection; 2724 Magnetospheric Physics: Magnetopause, cusp, and boundary layers; *KEYWORDS:* aurora, magnetic reconnection, cusp, magnetopause

1. Introduction

[2] There is considerable evidence that magnetic reconnection occurs at the Earth's magnetopause when the interplanetary magnetic field (IMF) B_z component is southward, zero, or northward. Most of this evidence consists of in situ measurements near the magnetopause. For example, field-aligned flows consistent with reconnection have been observed at the magnetopause at high latitudes, low latitudes, in the subsolar region, and on the flanks [e.g., *Sonnerup et al.*, 1981; *Gosling et al.*, 1991; *Paschmann et al.*, 1986; *Fuselier et al.*, 1991; *Kessel et al.*, 1996; *Phan et al.*, 2000]. Also consistent with reconnection, magnetic fields with a finite component normal to the magnetopause have been observed at several locations on the magnetopause [*Sonnerup et al.*, 1981].

[3] In addition to a substantial number of in situ measurements at the magnetopause, observations in the Earth's magnetospheric cusps are also consistent with magnetosheath plasma entry through reconnection [see *Smith and Lockwood*, 1996, and references therein]. Statistical analysis of ion and electron precipitation in the cusps shows that when the IMF is southward (northward), the highest-energy magnetosheath ions precipitate most equatorward (poleward). This time of flight or velocity filter effect is the direct result of an equatorward (poleward) limit to the open field lines that thread the cusp and the poleward (sunward) convection of newly reconnected field lines [e.g., *Onsager et al.*, 1993; *Smith and Lockwood*, 1996]. In addition to the B_z dependence on the cusp location and structure, there is also a B_y dependence that has been shown to be consistent with magnetic reconnection [*Newell et al.*, 1989; *Milan et al.*, 2000].

[4] The statistical location of the cusp for different IMF orientations can be understood reasonably well by assuming a simple picture of magnetic reconnection. In this simple picture, reconnection sites lie along a line (called the neutral line) where the magnetosheath and magnetospheric field lines are antiparallel. Antiparallel reconnection predicts that neutral lines will be poleward of the cusps at high latitudes when the IMF is northward. Furthermore, antiparallel reconnection predicts that the neutral line will be at low latitudes running across the dayside magnetopause for strictly southward IMF. When the IMF has a B_y component and B_z is negative, the reconnection line is at midlatitudes and not in the subsolar region [*Crooker*, 1979; *Luhmann et al.*, 1984].

[5] Although statistical studies suggest that antiparallel reconnection orders many observations, detailed properties of flows at the magnetopause for some events show deviations from this simple picture. In particular, some reconnection events for southward IMF with large B_y components have magnetic field shear angles across the magnetopause as low as 50° (instead of 180° predicted by antiparallel reconnection) [*Gosling et al.*, 1990]. Analysis and interpretation of ion and electron distributions for some reconnection events for northward IMF suggest that reconnection occurs equatorward of the cusp when the IMF is northward [*Onsager and Fuselier*, 1994; *Fuselier et al.*, 1997]. This equatorward reconnection must occur

[1]Lockheed Martin Advanced Technology Center, Palo Alto, California, USA.
[2]Space Sciences Laboratory, University of California, Berkeley, California, USA.
[3]Southwest Research Institute, San Antonio, Texas, USA.

0148-0227/02/2001JA900165$09.00

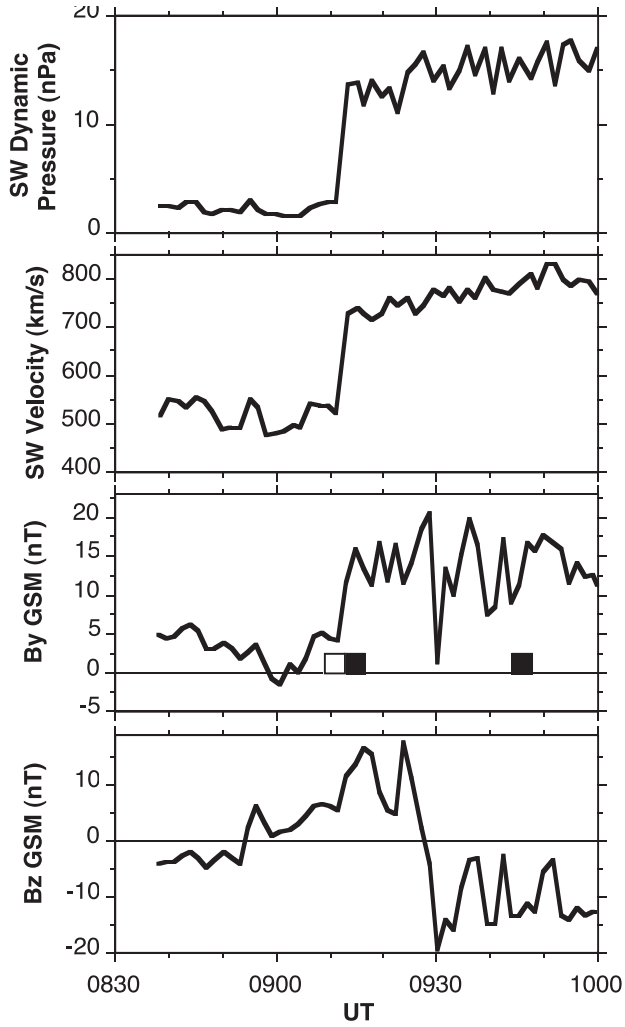

Figure 1. (top to bottom). Solar wind dynamic pressure, magnitude of the solar wind velocity, and the B_y and B_z GSM components of the interplanetary magnetic field (IMF) for data from the solar wind and magnetic field experiments on the Wind spacecraft 8 June 2000. The time has been shifted to account for propagation from the upstream spacecraft to the ionosphere. The solar wind velocity and dynamic pressure increase dramatically at the leading edge of an interplanetary shock. For the first ~20 min after the shock arrival in the ionosphere, the IMF was northward, then it turned southward. Squares in the B_y panel show time periods when the proton aurora is investigated.

on field lines that are not strictly antiparallel. Reconnection of field lines that are not strictly antiparallel is called component reconnection because only one component of the magnetosheath and magnetospheric fields is oppositely directed. There are significant differences between component and antiparallel reconnection, especially for southward IMF. In particular, component reconnection predicts that a neutral line runs across the dayside magnetosphere through the subsolar point when the IMF is southward (regardless of the magnitude of the B_y component). The B_y component determines the tilt of the neutral line relative to the equatorial plane.

[6] The combined in situ observations in the cusp and at the magnetopause have resulted in some ambiguities concerning reconnection. One ambiguity is the aforementioned interpretation of cusp and magnetopause observations using the antiparallel and component reconnection models. A second ambiguity is the length of the reconnection line. In situ measurements at a single magnetopause location and rapid traversals of the cusp by a spacecraft at a single longitude cannot be used to determine how much of the magnetopause is open at any one time. Two-spacecraft observations have helped [e.g., *Peterson et al.*, 1998; *Phan et al.*, 2000], but the overall length of the neutral line remains unknown. This length is one critical quantity needed to determine the total plasma transfer across the magnetopause.

[7] In this paper, a new observation technique is presented that allows global imaging of the ionospheric foot point of the cusp for any IMF orientation. Using this technique and tracing of magnetic field lines in a model magnetosphere, the length of the neutral line is estimated and the likelihood of component versus anti-parallel reconnection is investigated.

2. Observation Technique

[8] This paper uses observations from one of the Imager for Magnetopause to Aurora Global Exploration (IMAGE) Far Ultraviolet (FUV) imagers [*Mende et al.*, 2000]. The suite of FUV imagers provide the first global, simultaneous, and separate images of the proton and electron aurora. Image cadence and exposure is set by the spacecraft spin, with ~10-s exposures repeated every 2 min. The imager used here is the Spectrographic Imager (SI12), which images Doppler-shifted Lyman alpha emissions. These emissions are produced in the Earth's upper atmosphere by a charge exchange and deexcitation process. Energetic protons precipitating in the upper atmosphere collide with atoms and molecules and undergo charge exchange to neutral hydrogen. A fraction of this neutral hydrogen is in an excited state. Decay of the electron in the H atom from the excited

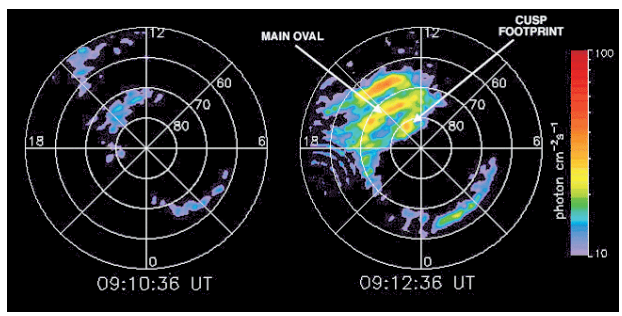

Figure 2. Consecutive proton aurora images (in magnetic local time-invariant latitude format) taken just before and just after the arrival of the interplanetary disturbance in the ionosphere. In response to this disturbance the proton aurora emissions increase dramatically in three distinct bands equatorward of, at, and poleward of the existing oval on the duskside. The spot located poleward of the oval is the ionospheric foot point of the cusp.

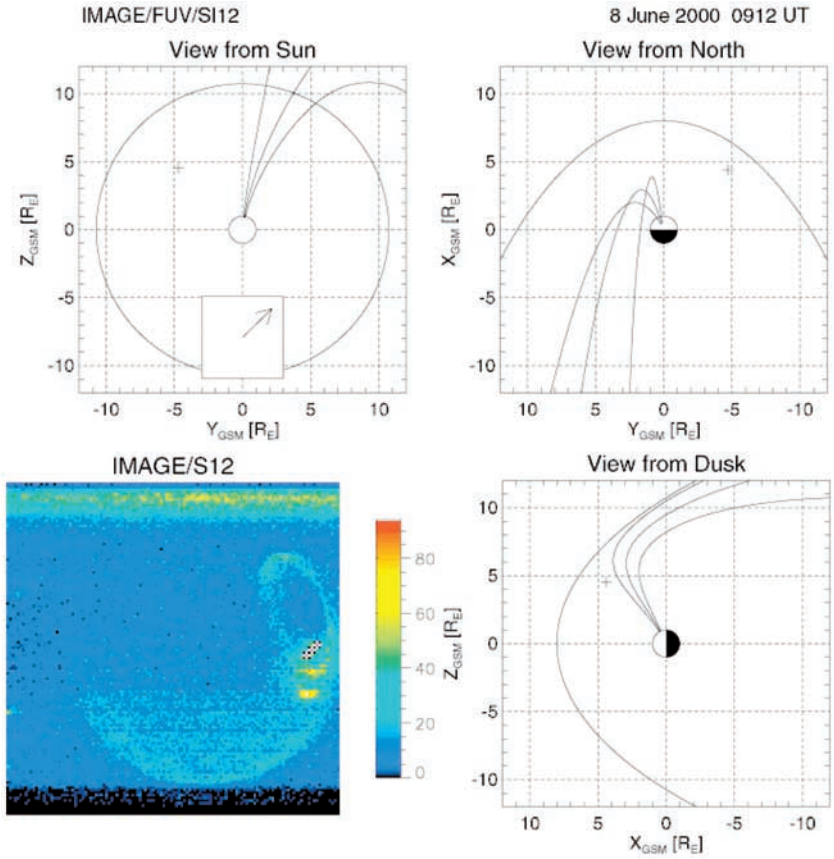

Figure 3. Proton aurora image from 0912 UT and three projected views of field line tracing in a model magnetic field. Three field lines were traced in the model magnetic field starting in the ionosphere surrounding the spot of proton aurora emissions poleward of the auroral oval (the ionospheric foot point of the cusp). In the top left-hand panel the square inset shows the IMF clock angle, the cross shows the location of the IMAGE spacecraft projected into the *Y-Z* plane, and the circle is the intersection of the model magnetopause with the terminator plane ($X = 0$). The three mapped field lines are lobe field lines that skim a narrow strip of the high-latitude, duskside magnetopause.

state to the ground state produces Lyman alpha emission. If the hydrogen atom is moving away from the SI12 imager, then the emissions are Doppler shifted toward wavelengths longer than 1216 Å. Precipitating protons can undergo this charge exchange and deexcitation process many times as they collide with the tenuous upper atmosphere. The multiple interactions with the atmosphere will produce a continuum of Doppler-shifted emissions at wavelengths extending from zero Doppler shift (i.e., 1215.67 Å) to the maximum Doppler shift determined by the energy of the incident proton.

[9] The near-Earth environment contains a high density of cold hydrogen, which produces the geocorona Lyman alpha. The SI12 was designed to eliminate this intense background source. This background (which could be >30 times more intense than the Lyman alpha produced by precipitating protons) is eliminated by using high spectral resolution (2 Å) and a "grill," which physically blocks the ~1216 Å Lyman alpha entering the spectrograph. As a result, the peak transmission is periodic, with the first transmission maximum at 1218 Å, the second at 1222 Å, etc. Transmission at 1218 Å corresponds to ~4 keV initial energy of the precipitating protons [*Gérard et al.*, 2000]. Instrument sensitivity to protons with energies of ~1 keV is only a few percent of its peak sensitivity.

[10] Because magnetosheath protons that precipitate in the cusp have typical energies of 1 keV, some special conditions must occur for the SI12 to observe cusp proton aurora. In general, solar wind dynamic pressures well above that in the nominal solar wind are required to produce sufficient emissions to be observed by SI12. The high solar wind dynamic pressure could be the result of a high solar wind density (which increases the proton flux at all energies) or a high solar wind velocity (which increases the proton flux above the average energy of 1 keV). Typically, cusp proton auroral emissions are observed when both of these conditions are met.

3. Observations

[11] An example of a high solar wind dynamic pressure interval on 8 June 2000 is shown in Figure 1. Data from the solar wind [*Ogilvie et al.*, 1995] and magnetic field [*Lepping et al.*, 1995] experiments on the Wind spacecraft are shown. Top to bottom are the solar wind dynamic pressure, the solar wind velocity, and the Y_{GSM} and Z_{GSM} components

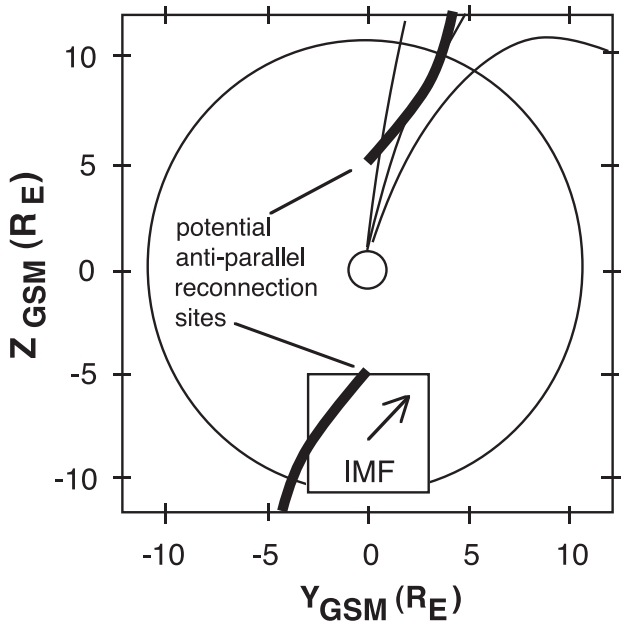

Figure 4. *Y-Z* projection of magnetic field lines mapped from the cusp foot point (from Figure 3) compared to the location for potential antiparallel reconnection sites. The field lines from the cusp foot point map to the region where antiparallel reconnection is expected to occur.

of the IMF. A coronal mass ejection (CME) shock is responsible for a large increase in the solar wind dynamic pressure. The time has been shifted to coincide with the arrival time of the effects of the CME shock wave in the ionosphere. These ionospheric effects are directly observable by the IMAGE SI12 (see below) and provide a direct and accurate (within the 2-min cadence of the images) measure of the timing between the observations on the Wind and IMAGE spacecraft. Because the Wind spacecraft was relatively near the Earth, this time shift was only ~10 min.

[12] Prior to 0912 UT, the solar wind dynamic pressure was near its nominal value of ~1.5 nPa. The solar wind velocity, already relatively high before 0912 UT, increased dramatically at 0912 UT. This velocity increase, combined with a substantial increase in the solar wind density (not shown) resulted in a more than a factor of 10 increase in the solar wind dynamic pressure. The IMF was approximately in the ecliptic plane prior to the arrival of the shock. The IMF immediately behind the shock had a large, positive B_y component and a large, positive B_z component. About 20 min after the shock arrival the IMF B_z component rotated southward, but the B_y component remained large and positive. The IMF B_x component (not shown) was small compared to the other two components during the interval. Three intervals in Figure 1 are marked by squares for detailed consideration.

[13] The effect on the ionosphere when the shock arrived is obvious in the invariant latitude-magnetic local time images in Figure 2 [from *Fuselier et al.*, 2001]. The left panel shows the SI12 proton aurora image at 0910 UT, prior to the shock arrival (i.e., the interval denoted by the open box in Figure 1). A part of a faint auroral oval is present near local noon. The right panel shows the next SI12 image, taken immediately after the shock arrival at 0912 UT. Significant brightening occurs in three bands near noon. These bands are poleward, at, and equatorward of the existing auroral oval seen in the first image. Although taken ~2 min apart, the exposure time for images from SI12 is only ~10 s. Thus there is very little time aliasing within a given auroral image. Of particular interest here is the spot located poleward of the oval. This spot has dimensions of 1–1.5 hours magnetic local time (MLT) and ~4° invariant latitude. Other emissions in this image are the subject of future analysis.

[14] Figure 3 shows the raw data format of the auroral image from Figure 2 at 0912 UT and a magnetic field line mapping of the spot from the ionosphere (at 100-km altitude) to the magnetosphere. The bright band across the top of the auroral image in the lower left-hand panel of Figure 3 is the intense geocoronal background that the SI12 imager must filter out. In this region of the image the spectrographic grating of the instrument is slightly detuned from its optimal performance and a small amount of geocoronal Lyman alpha leaks into the spectrograph. (This background is removed in Figure 2.) Clockwise around the auroral image are perspective views of three magnetic field lines in the Tsygenanko magnetic field model [*Tsygenanko*, 1995] projected into the *Y-Z*, *X-Y*, and *X-Z* GSM planes. Although the Tsygenanko field model is typically considered to be valid for dynamic pressures below 10 nPa, this model is used here under the assumption that the magnetopause and magnetospheric field lines on the dayside remain self-similar for pressures above 10 nPa. The field lines in the Tsygenanko field model are traced from three pixels in the SI12 image that surround the intense emissions in the spot poleward of the auroral oval. To better identify the pixels used in the field line tracing, each of the three pixels is located in the center of a 3 × 3 pixel, black on white, checkerboard square in the raw image. These three pixels are mapped from an invariant latitude of ~80° and MLT between 1300 and 1500. In each projection the cross shows the projected location of the IMAGE spacecraft. In the *X-Y* and *X-Z* projections the magnetopause location in the projection is shown. In the *Y-Z* projection the circle shows the intersection of the magnetopause with the terminator plane and the inset shows the IMF clock angle.

[15] The *Y-Z* projection (viewed from the sun) shows that the field lines map to the high-latitude duskside. The *X-Z* projection (viewed from dusk) shows that they follow the magnetopause, which is highly compressed owing to the high solar wind dynamic pressure. Actually, these field lines skim the magnetopause, but in this projection they appear to be inside the boundary. The *X-Y* projection (viewed from north) shows that these are lobe magnetic field lines that will may never cross the equatorial region or may cross it very far down the magnetotail.

[16] By draping the observed IMF field against the model magnetopause and comparing the orientation of the draped field with the field just inside the magnetopause from the magnetospheric model, the locations of potential anti-parallel reconnection sites are identified. Figure 4 reproduces the *Y-Z* projection of the mapped field lines in Figure 3 and compares these projected field lines with the projected locus of points where the magnetospheric

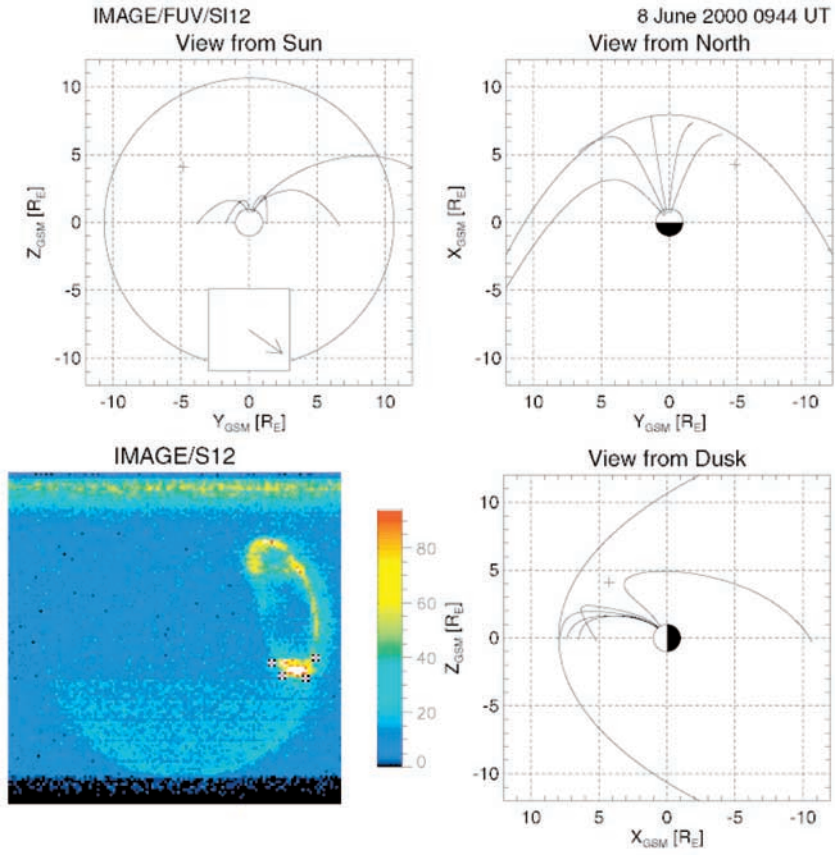

Figure 5. Same as Figure 3 for the proton aurora image taken at 0944 UT, when the IMF was southward with a large B_y component. In contrast to the proton aurora observations in Figure 3, there is no bright spot poleward of the auroral oval. However, the emissions in the vicinity of the dayside auroral oval have brightened considerably over a broad range of local time. The field lines from this broad region map to the magnetopause over a considerable local time range.

and draped IMF field lines are antiparallel. As seen in Figure 4, the field lines map out the fairly narrow region on the magnetopause where there is a high potential for antiparallel reconnection.

[17] Subsequent images from the SI12 (not shown) also exhibit a spot poleward of the auroral oval like the one in Figures 2 and 3. This spot persisted for as long as the IMF remained northward, and it remained approximately the same size. Figure 5 shows the raw data SI12 image and field line mapping at 0944 UT, when the IMF was southward. The format is the same as in Figure 3. The spot located poleward of the auroral oval has disappeared (as well as the spot equatorward of the oval) and the auroral oval in the vicinity of local noon has brightened and expanded. Actually, images from the time period between 0912 and 0944 UT (not shown) indicate a smooth progression as the IMF rotates from northward to southward. As the IMF rotates, the spot moves equatorward, merges with the existing auroral oval, brightens, and spreads out. The process of spreading out takes ~4–8 min. In Figure 5 the checkerboard squares are used to show 4 pixels used in the mapping. The mapped pixels are located at the equatorial edge of the bright region at ~70° invariant latitude and between 1100 and 1500 MLT. Field lines from these pixels map to the magnetopause over a broad region extending from tailward of the dusk terminator to the dawnside near 0900 LT.

[18] Figure 6 shows the *Y-Z* projection of the mapped field lines in Figure 5 and compares these field lines with the locus of points where the magnetospheric and draped magnetosheath lines are antiparallel. In contrast to the northward IMF interval in Figure 4 the field lines mapped from the broad region of intense emissions at the auroral oval do not appear to intersect the magnetopause at regions where the magnetosheath and magnetospheric field lines are antiparallel. In particular, there are emissions at the foot point of field lines that map to near the subsolar region.

[19] Figure 7 shows the solar wind [*Frank et al.*, 1994] and magnetic field [*Kokubun et al.*, 1994] data from the Geotail spacecraft from just upstream of the bow shock during another high solar wind dynamic pressure interval. The format is the same as in Figure 1. Unlike the interval in Figure 1, the interval in Figure 7 is not associated with an interplanetary shock. Rather, it is simply an interval when the solar wind dynamic pressure is relatively high, but the solar wind velocity is only ~10% higher than its nominal value of ~400 km/s. A northward IMF and a southward IMF interval are marked for detailed investigation. Because this interval is not associated with a rapid change in dynamic pressure, the timing between the solar wind

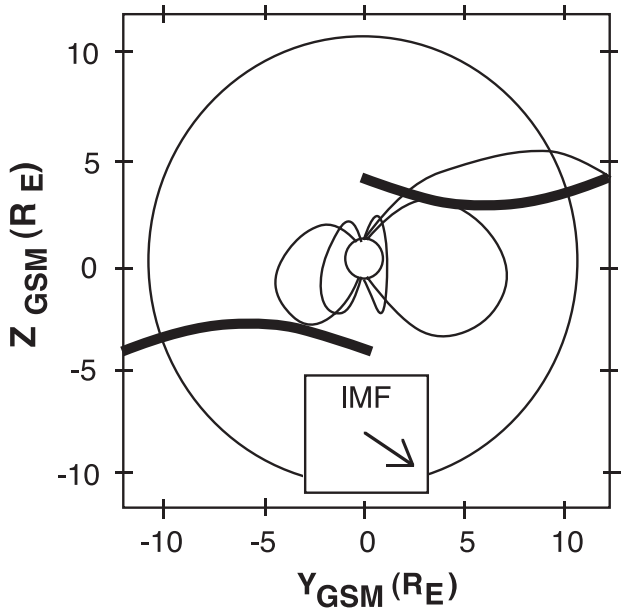

Figure 6. *Y-Z* projection of the mapped magnetic field lines (from Figure 5) from the broad region of cusp emissions compared to the location for potential antiparallel reconnection sites. The field lines from the cusp do not coincide with those field lines where antiparallel reconnection is expected to occur.

monitor and the effects in the ionosphere was more difficult to estimate. In particular, the computed propagation time to the ionosphere (convecting the solar wind from the location of the Geotail spacecraft to the bow shock at the solar wind speed and through the magnetosheath, across the magnetopause and to the ionosphere using half the solar wind speed) was not sufficient to associate the north to south IMF rotations with changes in the proton aurora. (Geotail was located in the solar wind near the terminator so a solar wind disturbance observed at Geotail arrives in the ionosphere only 1 min later, using this approximate formula.) Additional time (~7 min) was needed to align north to south transitions of the IMF with changes in the aurora. This may be evidence for a reconfiguration time in the ionosphere [see *Ridley et al.*, 1999; *Lockwood and Cowley*, 1999]. This subject requires further detailed investigation, including analysis of more events, and is beyond the scope of this paper.

[20] Figure 8 shows SI12 images in invariant latitude-magnetic local time format for the two periods of interest that are identified in Figure 7. The format for Figure 8 is similar to that of Figure 2. The image at 1159:50 UT was taken when the IMF was northward but transitioning to southward. The image at 1210:03 UT was taken when the IMF was southward.

[21] Similar to Figures 2 and 3, the image taken during the northward IMF interval shows a spot poleward of the oval at ~80° invariant latitude and 1400 MLT. Another spot is seen at 1200 MLT on the auroral oval, and there is also considerable auroral activity on the duskside between 60° and 80° invariant latitude.

[22] The activity on the duskside is probably associated with ring current proton precipitation and extends to high latitudes because the IMF is northward. The duskside emissions poleward of the oval are weaker at 1210:03 UT, when the IMF was southward. The spot at 80° invariant latitude and 1400 MLT is identified as the cusp. As the IMF turns southward, this spot was observed to move equatorward and merge with the spot near 1200 MLT on the auroral oval and then spread out in MLT. The result of this transformation is the intense emissions near 1200 MLT on the auroral oval in the image taken at 1210:03 UT.

[23] Figure 9 shows the SI12 image and field line mapping at 1159 UT, when the IMF was northward, just before it turned southward. The format for Figure 9 is the same as in Figures 3. For the interval in Figure 7, IMAGE spacecraft was much closer to the Earth than for the interval in Figure 1. The auroral oval in the top left-hand panel of Figure 9 covers nearly the entire SI12 field of view. The Sun direction is toward the lower right-hand corner of the image. Although there is considerable proton

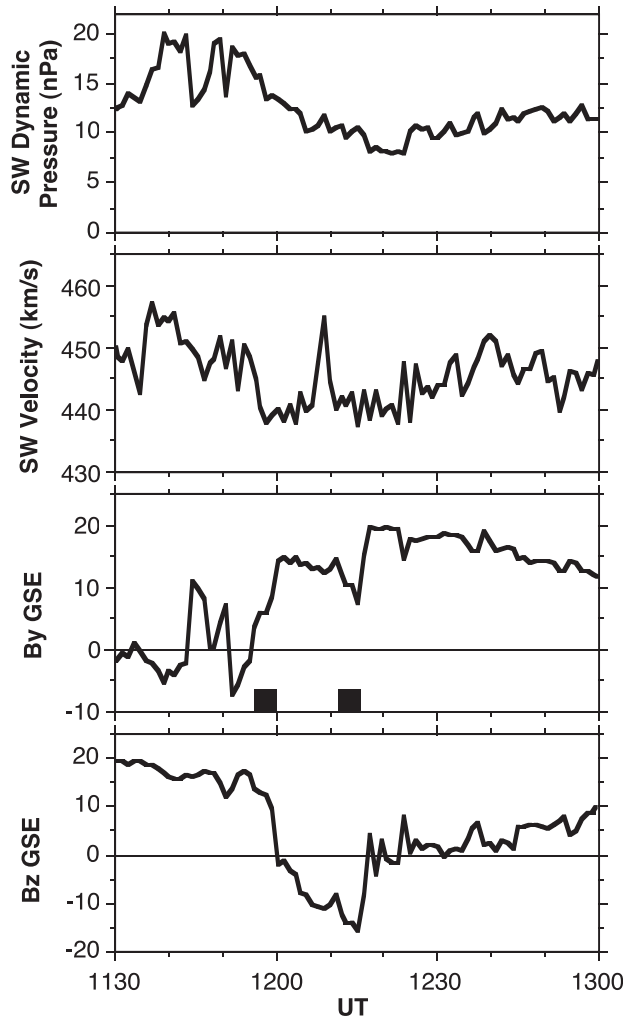

Figure 7. Interval of high solar wind dynamic pressure for solar wind and magnetic field data from the Geotail spacecraft on 28 July 2000 The format is the same as in Figure 1. For the first part of the interval the IMF is northward. Later, the IMF turns southward but has a large B_y component. Two periods of proton aurora observations are identified in the B_y component panel.

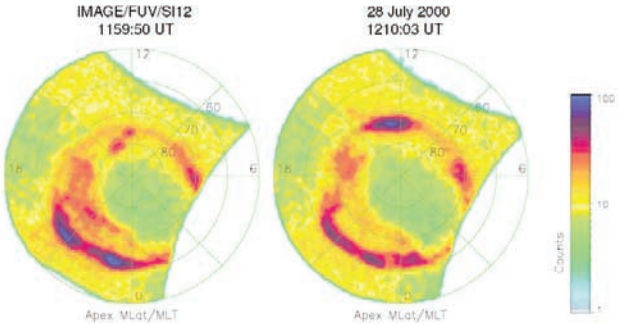

Figure 8. Proton aurora images (in magnetic local time-invariant latitude format) taken when the IMF was northward (1159:50 UT) and southward (1210:03 UT). The ionospheric foot point of the cusp is the spot located poleward of the oval at ~79° invariant latitude and 1400 MLT in the image from 1159:50 UT. As the IMF rotates from north to south, this spot moves equatorward, merges with the spot near noon, intensifies, and spreads in MLT. The result, after the IMF has turned southward, is the image from 1210:03 UT.

aurora poleward of the oval on the duskside, there is also a spot near local noon that is poleward of, and separated from, the auroral oval. Three center pixels in the checkerboard squares show the location of field lines that are mapped from the ionosphere. The pixels mapped were located on the poleward edge of the spot at 81° invariant latitude and between 1300 and 1500 MLT. These pixels map to the lobe on the duskside, high-latitude magnetopause. In this region the lobe field lines and the draped magnetosheath field lines are anti-parallel, since the IMF is northward with a large B_y component (Figure 7 and the inset in the *Y-Z* projection in Figure 9).

[24] Although there is some variability due to changes in the solar wind dynamic pressure and IMF B_y component, the spot that is poleward of the auroral oval in Figure 9 is observed in other SI12 images (not shown) during the interval when the IMF is northward. Figure 10 shows the SI12 image and field line mapping at 1210 UT, after the IMF is southward. The format is the same as in Figure 3. Comparing the proton aurora in Figures 9 and 10, it is apparent that the spot poleward of the aurora oval has disappeared and the auroral oval approximately on

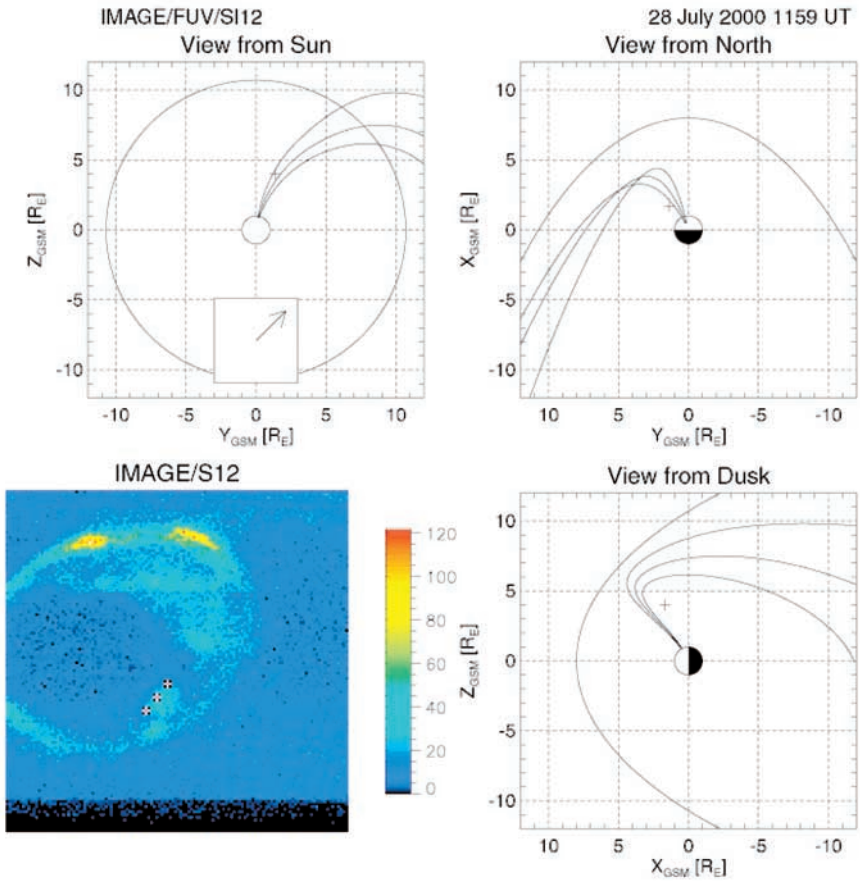

Figure 9. Proton aurora and field line mapping from the northward IMF interval in Figure 7. The format is the same as in Figure 3. The spot poleward of the oval maps to the duskside, high-latitude magnetopause. This is consistent with the location of potential antiparallel reconnection sites because of the positive B_y component of the IMF.

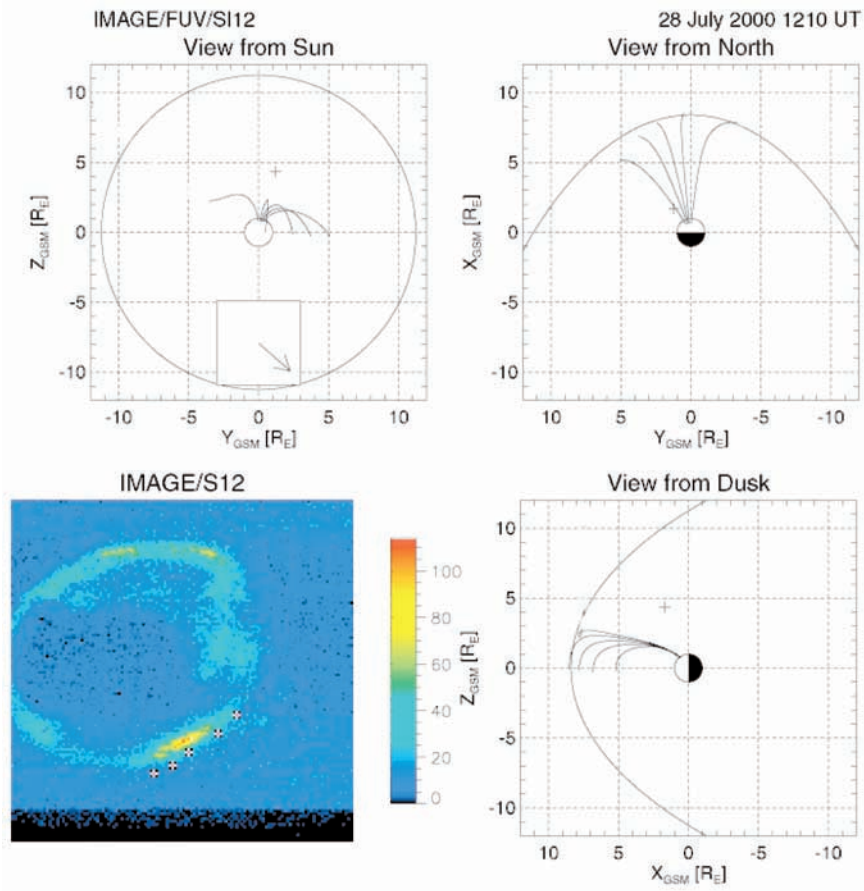

Figure 10. Proton aurora and field line mapping from the southward IMF interval in Figure 7. The format is the same as in Figure 3. For southward IMF, there is no longer any spot poleward of the auroral oval on the dayside near noon. This spot is replaced by a region of proton emissions extending over a broad range of local time centered on local noon. Field lines from this region of emissions map to the dayside magnetopause over a considerable range of local time.

either side of local noon has brightened significantly. The pixels identified on the equatorial edge of this bright region lie along ~70° invariant latitude and between 1100 and 1500 MLT. They map to the dayside equatorial plane, intersecting the dayside magnetopause over a local time range from ~0900 to 1500 LT. As in the first event (Figure 5), the IMF has a large B_y component and B_z was negative, yet auroral emissions are seen continuously across local noon. These emissions at local noon in Figure 10 map to the subsolar region.

4. Discussion

[25] Dayside proton aurora emissions in this paper show distinct differences for northward and southward IMF. For northward IMF, there is a spot of emissions poleward of the auroral oval. For southward IMF the spot is not present but the auroral oval near local noon is bright over a wide range of local time centered on noon.

[26] Previous study of auroral emissions used FUV wavelengths that do not separate emissions produced by electron and proton precipitation. A bright spot in the LBH emissions at 1400–1600 Å was observed poleward of the auroral oval when the IMF was northward [*Milan et al.*, 2000]. The location of this spot depended on the IMF B_y component. When the IMF B_y component was positive (negative), the emissions were located at post-noon (pre-noon) local time. When the IMF turned southward, the bright spot of auroral emissions disappeared. This previous study interpreted these observations as aurora created by precipitating electrons in the cusp.

[27] Observations in Figures 3 and 9 are consistent with these previous results. In Figures 3 and 8 the IMF B_z and B_y components are positive and the proton aurora emissions occur in the post-noon sector in a fairly localized spot that is poleward of the auroral oval. Consistent with the previous study, this spot is interpreted here as the foot point of the cusp. Furthermore, Figures 5 and 10 show that when the IMF B_z component is negative, there is no longer any spot located poleward of the auroral oval.

[28] On the basis of the magnetic reconnection at the magnetopause, Figure 4 offers an interpretation of the location of the cusp aurora for northward IMF. When traced to the magnetosphere, the field lines at the poleward edge of the cusp aurora are consistent with the fairly narrow region on the magnetopause where the draped magnetosheath magnetic field and the magnetospheric magnetic fields are antiparallel. The poleward edge of the spot is chosen for the

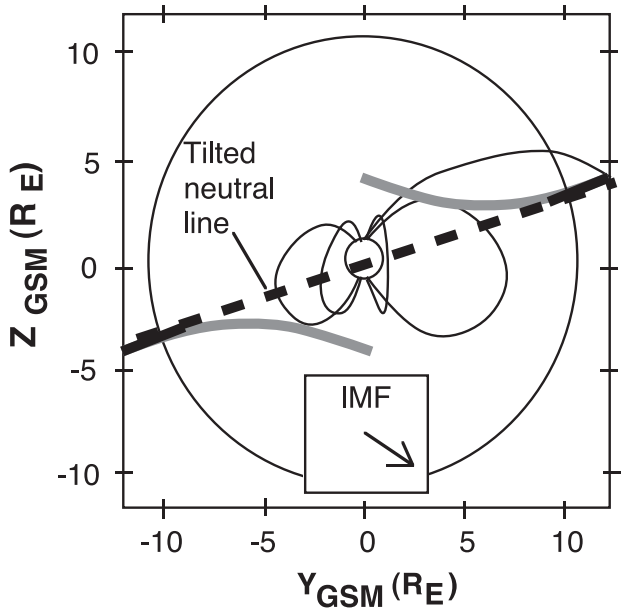

Figure 11. Proton aurora emissions observed during southward IMF (Figures 5 and 9) are consistent with a tilted neutral line that passes through the subsolar region. This tilted neutral line is predicted by the component reconnection model.

field line tracing because the SI12 imager is sensitive to high-energy (~>1 keV) protons and, according to the velocity filter effect [e.g., *Onsager et al.*, 1993] and previous in situ cusp observations [*Woch and Lundin*, 1992], these protons will precipitate most poleward for northward IMF.

[29] As the IMF turned southward, previous observations showed that cusp aurora emissions moved equatorward, faded, and disappeared [*Milan et al.*, 2000]. These previous observations were made with an imager that could not separate proton and electron emissions. In contrast to these previous observations, proton aurora observations in this paper show that the cusp precipitation merges with the existing auroral oval and that the intensity and local time extent of the emissions increases. The differences in the two results are likely due to differences in imaging techniques and possibly the type of event that was imaged. The previous study used ultraviolet emissions produced by both electron and proton precipitation, with no way to distinguish the two emissions. Thus it is not possible to determine if the proton flux during the events was sufficient to produce LBH emissions. The study presented here uses emissions produced only by proton precipitation [*Mende et al.*, 2001] during events when the proton flux was very high.

[30] Mapping the equatorial edge of these intense proton aurora emissions from the ionosphere to the magnetosphere, it is apparent in Figures 5 and 10 that they are consistent with a reconnection region that extends across most of the dayside magnetopause. The equatorial edge of the broad emissions is chosen for the field line tracing because the SI12 imager is most sensitive to high-energy (~>1 keV) protons and, according to the velocity filter effect [e.g., *Onsager et al.*, 1993], these protons will precipitate most equatorward for southward IMF. These results have implications on the amount of plasma transfer at the magnetopause and the type of reconnection that is occurring for southward IMF.

[31] The significant local time extent of the cusp precipitation for southward IMF is consistent with a magnetopause that is open over nearly the entire dayside. From Figures 5 and 10 it is estimated that the length of the neutral line is between 20 and 25 R_E and ~10 R_E, respectively. In contrast, there is a narrow local time extent of cusp precipitation for northward IMF. From Figure 4 it is estimated that the neutral line is only ~5 R_E long. These differences will lead to differences in the plasma transfer rate across the magnetopause. To make a quantitative determination of these differences, the reconnection rate must be known at each point on the magnetopause. This rate cannot be obtained from the cusp aurora observations in this paper. However, for a constant rate the larger local time extent of the reconnection neutral line for southward IMF will result in a 2–5 times higher total plasma transfer than that for northward IMF.

[32] The field lines mapped from the equatorial edge of the cusp emissions for southward IMF are compared with the predictions for antiparallel reconnection in Figure 6. The results indicate that the broad local time of the mapped field lines and their extent on either side of the subsolar region are inconsistent with the location of antiparallel reconnection sites on the dayside magnetopause. In particular, the antiparallel reconnection sites occur at midlatitudes and do not extend smoothly across the subsolar point. In contrast, the brightest cusp aurora emissions are seen near local noon in Figures 5 and 10. Figure 11 shows how a modification of the reconnection model that allows a tilted neutral line, consistent with component reconnection on the dayside, is consistent with the local time extent and subsolar nature of the cusp precipitation in Figures 5 and 10.

[33] The degree to which the observations are consistent with antiparallel reconnection for northward IMF and component reconnection for southward IMF is surprising. For northward IMF the antiparallel reconnection line is well correlated with the field lines that map from the narrow cusp foot point in Figure 4. In contrast, subsolar reconnection would occur between magnetosheath and magnetospheric magnetic field lines that had only ~40° and 45° shear for the southward IMF orientations in Figures 5 and 10, respectively. This is close to the minimum shear angles reported for in situ observations of reconnection events at the magnetopause for southward IMF [*Gosling et al.*, 1990].

[34] The discrepancy between the proton aurora observations and predictions from antiparallel reconnection is not likely to be resolved by improvements in the magnetic field model used to trace the magnetic field lines from the ionosphere to the magnetopause. A more accurate magnetospheric magnetic field model also will predict a region around the subsolar region where reconnection must occur at midlatitudes for southward IMF and a large B_y component. An interesting reconciliation of the observations for northward and southward IMF is the suggestion that component reconnection is occurring in the subsolar region for both northward IMF and southward IMF. Observations at the magnetopause and in the cusp have indicated the possibility of component reconnection for northward IMF

[*Onsager and Fuselier*, 1994; *Fuselier et al.*, 1997; *Chandler et al.*, 1999; *Fuselier et al.*, 2000] as well as for southward IMF [*Gosling et al.*, 1990]. It may be that proton aurora emissions in the vicinity of the auroral oval near local noon during northward IMF (see Figures 3 and 9) are consistent with component reconnection. (These field lines map to the subsolar region.) Further analysis of the SI12 observations is needed to confirm this possibility.

[35] **Acknowledgments.** Solar wind observations in this paper are from the CDAWeb. The authors thank R. P. Lepping, K. W. Ogilvie, L. A. Frank, and S. Kokubun for providing the key parameter data. Research at Lockheed Martin was supported by an IMAGE data analysis subcontract (PPB00533) from the University of California, Berkeley. Research at the University of California, Berkeley was supported by an IMAGE data analysis contract from Southwest Research Institute.

[36] Hiroshi Matsumoto thanks S. Kokubun and H. Fukunishi for their assistance in evaluating this paper.

References

Chandler, M. O., S. A. Fuselier, M. Lockwood, and T. E. Moore, Evidence of component merging equatorward of the cusp, *J. Geophys. Res.*, *104*, 22,623, 1999.

Crooker, N., Dayside merging and cusp geometry, *J. Geophys. Res.*, *84*, 951, 1979.

Frank, L. A., K. L. Ackerson, W. R. Paterson, J. A. Lee, M. R. English, and G. L. Pickett, The comprehensive plasma instrumentation (CPI) for the GEOTAIL spacecraft, *J. Geomagn. Geoelectr.*, *46*, 23, 1994.

Fuselier, S. A., D. M. Klumpar, and E. G. Shelley, Ion reflection and transmission during reconnection at the Earth's subsolar magnetopause, *Geophys. Res. Lett.*, *18*, 139, 1991.

Fuselier, S. A., B. J. Anderson, and T. G. Onsager, Electron and ion signatures of field line topology at the low–shear magnetopause, *J. Geophys. Res.*, *102*, 4847, 1997.

Fuselier, S. A., K. J. Trattner, and S. M. Petrinec, Cusp observations of high- and low-latitude reconnection for northward IMF, *J. Geophys. Res.*, *105*, 253, 2000.

Fuselier, S. A., A. G. Ghielmetti, T. E. Moore, M. R. Collier, J. M. Quinn, G. R. Wilson, P. Wurz, S. B. Mende, H. U. Frey, C. Jamar, J.-C. Gerard, and J. L. Burch, Ion outflow observed by IMAGE: Implications for source regions and heating mechanisms, *Geophys. Res. Lett.*, *28*, 1163, 2001.

Gérard, J.-C., B. Hubert, D. V. Bisikalo, and V. I. Shematovich, A model of the Lyman-alpha line profile in the proton aurora, *J. Geophys. Res.*, *105*, 15,795, 2000.

Gosling, J. T., M. F. Thomsen, S. J. Bame, R. C. Elphic, and C. T. Russell, Plasma flow reversals at the dayside magnetopause and the origin of asymmetric polar cap convection, *J. Geophys. Res.*, *95*, 8073, 1990.

Gosling, J. T., M. F. Thomsen, S. J. Bame, R. C. Elphic, and C. T. Russell, Observations of reconnection of interplanetary and lobe magnetic field lines at the high-latitude magnetopause, *J. Geophys. Res.*, *96*, 14,097, 1991.

Kessel, R. L., S.-H. Chen, J. L. Green, S. F. Fung, S. A. Boardsen, L. C. Tan, T. E. Eastman, J. D. Craven, and L. A. Frank, Evidence of high-latitude reconnection during northward IMF: Hawkeye observations, *Geophys. Res. Lett.*, *23*, 583, 1996.

Kokubun, S., T. Yamamoto, M. H. Acuña, K. Hayashi, K. Shirokawa, and H. Kawano, The Geotail magnetic field experiment, *J. Geomagn. Geoelectr.*, *46*, 7, 1994.

Lepping, R. P., et al., The wind magnetic field investigation, in *The Global Geospace Mission*, edited by C. T. Russell, p. 207, Kluwer Acad., Norwell, Mass., 1995.

Lockwood, M., and S. W. H. Cowley, Comment on "A statistical study of the ionospheric convection response to changing interplanetary magnetic field conditions using the assimilative mapping of ionospheric electrodynamics technique" by A. J. Ridley et al., *J. Geophys. Res.*, *104*, 4387, 1999.

Luhmann, J. G., R. J. Walker, C. T. Russell, N. U. Crooker, J. R. Spreiter, and S. S. Stahara, Patterns of potential magnetic field merging sites on the dayside magnetopause, *J. Geophys. Res.*, *89*, 1739, 1984.

Mende, S. B., et al., Far ultraviolet imaging from the IMAGE spacecraft, 3, Spectral imaging of Lyman-alpha and OI 135.6 nm, *Space Sci. Rev.*, *91*, 271, 2000.

Mende, S. B., H. U. Frey, M. Lampton, J.-C. Gerard, B. Hubert, S. Fuselier, J. Spann, R. Gladstone, and J. L. Burch, Global observations of proton and electron auroras in a substorm, *Geophys. Res. Lett.*, *28*, 1139, 2001.

Milan, S. E., M. Lester, S. W. H. Cowley, and M. Brittnacher, Dayside convection and auroral morphology during an interval of northward interplanetary magnetic field, *Ann. Geophys.*, *18*, 436, 2000.

Newell, P. T., C.-I. Meng, D. G. Sibeck, and R. Lepping, Some low-altitude cusp dependencies on the interplanetary magnetic field, *J. Geophys. Res.*, *94*, 8921, 1989.

Ogilvie, K. W., et al., A comprehensive plasma instrument for the Wind spacecraft, in *The Global Geospace Mission*, edited by C. T. Russell, p. 55, Kluwer Acad., Norwell, Mass., 1995.

Onsager, T. G., and S. A. Fuselier, The location of magnetic reconnection for northward and southward interplanetary magnetic field, in *Solar System Plasmas in Space and Time, Geophys. Monogr. Ser.*, vol. 84, edited by J. L. Burch and J. H. Waite Jr., p. 183, AGU, Washington, D. C., 1994.

Onsager, T. G., C. A. Kletzing, J. B. Austin, and H. MacKiernan, Model of magnetosheath plasma in the magnetosphere: Cusp and mantle particles at low altitudes, *Geophys. Res. Lett.*, *20*, 479, 1993.

Paschmann, G., I. Papamastorakis, W. Baumjohann, N. Sckopke, C. W. Carlson, B. U. O. Sonnerup, and H. Luhr, The magnetopause for large magnetic shear: AMPTE/IRM observations, *J. Geophys. Res.*, *91*, 11,099, 1986.

Peterson, W. K., et al., Simultaneous observations of solar wind plasma entry from FAST and POLAR, *Geophys. Res. Lett.*, *25*, 2081, 1998.

Phan, T. D., et al., Extended magnetic reconnection at the Earth's magnetopause from detection of bi-directional jets, *Nature*, *404*, 848, 2000.

Ridley, A. J., G. Lu, C. R. Clauer, and V. O. Papitashvili, Reply, *J. Geophys. Res.*, *104*, 4393, 1999.

Smith, M. F., and M. Lockwood, Earth's magnetospheric cusps, *Rev. Geophys.*, *34*, 233, 1996.

Sonnerup, B. U. O., Magnetopause reconnection rate, *J. Geophys. Res.*, *79*, 1546, 1974.

Sonnerup, B. U. Ö., G. Paschmann, I. Papamastorakis, N. Sckopke, G. Haerendel, S. J. Bame, J. R. Asbridge, J. T. Gosling, and C. T. Russell, Evidence for magnetic field reconnection at the Earth's magnetopause, *J. Geophys. Res.*, *86*, 10,049, 1981.

Tsyganenko, N. A., Modeling the Earth's magnetospheric magnetic field confined within a realistic magnetopause, *J. Geophys. Res.*, *100*, 5599, 1995.

Woch, J., and R. Lundin, Magnetosheath plasma precipitation in the polar cusp and its control by the interplanetary magnetic field, *J. Geophys. Res.*, *97*, 1421, 1992.

J. L. Burch, Southwest Research Institute, San Antonio, TX 78228, USA.

H. U. Frey and S. B. Mende, Space Sciences Laboratory, University of California, Berkeley, CA 94720, USA.

S. A. Fuselier and K. J. Trattner, Lockheed Martin Advanced Technology Center, Palo Alto, CA 94304, USA. (fuselier@spasci.com)